Nuclear cusps and singularities in the nonadditive kinetic potential bifunctional from analytical inversion

Mojdeh Banafsheh [1,*] Tomasz A. Wesolowski [2,†] Tim Gould [3,‡] Leeor Kronik [4,§] and David A. Strubbe [1,¶]

[1]*Department of Physics, University of California, Merced, Merced, California 95348, USA*

[2]*Département de Chimie Physique 30, Université de Genève, Quai Ernest-Ansermet, CH-1211 Genève 4, Switzerland*

[3]*Queensland Micro and Nanotechnology Centre, Griffith University, Nathan, Queensland 4111, Australia*

[4]*Department of Molecular Chemistry and Materials Science, Weizmann Institute of Science, Rehovoth 76100, Israel*

(Received 1 July 2022; accepted 29 September 2022; published 17 October 2022)

The nonadditive kinetic potential v^{NAD} is a key quantity in density-functional theory (DFT) embedding methods, such as frozen density embedding theory and partition DFT. v^{NAD} is a bifunctional of electron densities ρ_{B} and $\rho_{\mathrm{tot}} = \rho_{\mathrm{A}} + \rho_{\mathrm{B}}$. It can be evaluated using approximate kinetic-energy functionals, but accurate approximations are challenging. The behavior of v^{NAD} in the vicinity of the nuclei has long been questioned, and singularities were seen in some approximate calculations. In this article, the existence of singularities in v^{NAD} is analyzed analytically for various choices of ρ_{B} and ρ_{tot}, using the nuclear cusp conditions for the density and Kohn-Sham potential. It is shown that no singularities arise from smoothly partitioned ground-state Kohn-Sham densities. We confirm this result by numerical calculations on diatomic test systems HeHe, $HeLi^+$, and H_2, using analytical inversion to obtain a numerically exact v^{NAD} for the local density approximation. We examine features of v^{NAD} which can be used for development and testing of approximations to $v^{\mathrm{NAD}}[\rho_{\mathrm{B}}, \rho_{\mathrm{tot}}]$ and kinetic-energy functionals.

DOI: 10.1103/PhysRevA.106.042812

I. INTRODUCTION

When the precise description of large and complex systems is not affordable computationally, they can be partitioned into smaller subsystems to make the calculations feasible. The main quantities of interest often pertain only to a localized region of the whole system. Such a region can be solved separately, with a higher level of theory that is more computationally costly, while the the rest of the system can be solved with computationally cheaper methods [1,2]. Examples of this embedding strategy include chromophores in protein environments or an aqueous solution [3], electrolyte molecules in solvents [4], organic molecules in aggregates [5], quantum defects in solids [6], or ions in a plasma with an average-atom model [7].

Two appealing methods for calculating the electronic structure of complex molecular systems in the framework of density-functional theory (DFT) are frozen-density embedding theory (FDET) [8–11] and partition DFT [12,13]. They allow the total electronic density to be divided into subsystem densities that can be separately calculated in a formally exact framework.

In calculations based on system-fragmenting methods within the Kohn-Sham DFT framework or quantum mechanics combined with molecular mechanics (QM/MM) [3] approaches, the relation between the potential of two subsystems is investigated via the so-called nonadditive kinetic potential functional $v^{\mathrm{NAD}}[\rho_{\mathrm{B}}, \rho_{\mathrm{tot}}]$ [14]. This quantity plays a critical role in calculating the correct ground-state density. In the overlap regions between partitioned densities, v^{NAD} takes into account the orthogonality of the wave functions of the full system (but not between subsystems [15]).

v^{NAD} can be evaluated through a kinetic-energy functional [8,11], as a "decomposable approximation"; the semi-local one most commonly used for v^{NAD} was introduced in [16] and tested comprehensively in [17]. The simple Thomas-Fermi and von Weizsäcker functionals are found to perform very poorly [15]. In general kinetic-energy functionals [18,19] are at a much cruder state of development than exchange-correlation functionals and perform poorly for v^{NAD}. They can be used for orbital-free DFT [20], but continue to be an area of active investigation [21–23]. To go beyond semi-local approximations, v^{NAD} can be evaluated for real systems through somewhat problematic numerical inversion [15,24–26], or "nondecomposable" approximations, specifically for v^{NAD} [27,28].

DFT approximations are evaluated by their capacity to provide well-known properties of the ground state with high accuracy. The cusp relation (or cusp condition) states that for Coulomb potentials, the electron density has a cusp at the position of the nuclei. In DFT-related approaches, the cusp relations [29–33] are an important property of an accurately calculated ground-state density and have corresponding singularities in the Kohn-Sham potential. Whether $v^{\mathrm{NAD}}[\rho_{\mathrm{B}}, \rho_{\mathrm{tot}}]$ should have such singularities due to nuclear cusps, and

*mbanafsheh@ucmerced.edu
†tomasz.wesolowski@unige.ch
‡t.gould@griffith.edu.au
§leeor.kronik@weizmann.ac.il
¶dstrubbe@ucmerced.edu

whether any approximations produce them, has been unclear. A preliminary investigation with analytic inversion suggested that there were singularities in $v^{\mathrm{NAD}}[\rho_{\mathrm{B}}, \rho_{\mathrm{tot}}]$ for diatomic systems [14]. However, the following questions remain open: Does $v^{\mathrm{NAD}}[\rho_{\mathrm{B}}, \rho_{\mathrm{tot}}]$ contain singularities at the nuclei for any admissible [14] pair of densities ρ_{B} and ρ_{tot} in any Coulomb system? Does $v^{\mathrm{NAD}}[\rho_{\mathrm{B}}, \rho_{\mathrm{tot}}]$ present any other discontinuities? If yes, how are they related to the ground-state charge density? The presence of singularities is important as a test for v^{NAD} approximations and potentially to know whether such features pose a numerical challenge in using v^{NAD} for embedding calculations. Correct reproduction of the kinetic-energy density or v^{NAD} features around nuclei can be essential to avoid artificial charge leaks from the nuclei to the environment [27] and for calculations of properties involving core electrons, including light elements, x-ray spectra, or warm dense matter in which core orbitals overlap between atoms at high pressure [34,35].

In this article, we theoretically prove the nonexistence at the vicinity of the nuclei of singularities in analytically inverted $v^{\mathrm{NAD}}[\rho_{\mathrm{B}}, \rho_{\mathrm{tot}}]$ from a class of densities that weakly overlap in space and we show consistent numerical results for model systems. Section II reviews the nonadditive potential bifunctional and how it can be constructed from analytical inversion. The setup for a specific class of densities for which the inverted potential is free of cusp-like singularities is explained and we conclude the cases for which singularities at the vicinity of the nuclei are expected. Section III gives details of how numerical calculations of analytically inverted $v^{\mathrm{NAD}}[\rho_{\mathrm{B}}, \rho_{\mathrm{tot}}]$ were carried out for various partitionings of ground-state Kohn-Sham densities. In Sec. IV we present results for the diatomic model systems HeHe, $HeLi^+$, and H_2 with comparison to calculations from the von Weizsäcker kinetic functional [36]. We examine the features found in the analytically inverted v^{NAD}. Two Appendixes provide more detailed mathematical analysis of the smooth parts of densities and potentials and the relation of cusps in densities and singularities in potentials.

II. THEORY

We assume finite molecular systems throughout this work. Consider a system described by the DFT Kohn-Sham equations (in atomic units)

$$\left[-\tfrac{1}{2}\nabla^2 + v_{\mathrm{KS}}[\rho](\mathbf{r})\right]\phi_i(\mathbf{r}) = \epsilon_i\phi_i(\mathbf{r}), \tag{1}$$

where ρ is the electronic charge density, ϕ_i is a Kohn-Sham orbital, and ϵ_i is the corresponding Kohn-Sham eigenvalue. The Kohn-Sham potential is

$$v_{\mathrm{KS}}[\rho](\mathbf{r}) := v_{\mathrm{ext}}(\mathbf{r}) + v_{\mathrm{Hxc}}[\rho](\mathbf{r}), \tag{2}$$

where $v_{\mathrm{Hxc}}[\rho](\mathbf{r}) := \frac{\delta E_{\mathrm{Hxc}}}{\delta\rho}$ is the Hartree, exchange, and correlation (Hxc) potential obtained exactly or via an approximation.

The density is given by

$$\rho(\mathbf{r}) := \sum_i f_i|\phi_i(\mathbf{r})|^2, \tag{3}$$

where f_i is the occupation factor of orbital ϕ_i. In frozen-density embedding theory [1], we regard the system as divided into subsystems j. The ground-state solution for each is obtained by Kohn-Sham equations for its orbitals i:

$$\left[-\tfrac{1}{2}\nabla^2 + v_{\mathrm{KS}}[\rho_j](\mathbf{r}) + v_{\mathrm{emb}}[\rho, \rho_j](\mathbf{r})\right]\phi_{ij}(\mathbf{r}) = \epsilon_{ij}\phi_{ij}(\mathbf{r}), \tag{4}$$

where the embedding potential is

$$v_{\mathrm{emb}}[\rho, \rho_j](\mathbf{r}) = v_{\mathrm{KS}}[\rho](\mathbf{r}) - v_{\mathrm{KS}}[\rho_j](\mathbf{r}) + \frac{\delta T_s[\rho]}{\delta\rho(\mathbf{r})} - \frac{\delta T_s[\rho_j]}{\delta\rho_j(\mathbf{r})}. \tag{5}$$

This formulation relies on the assumption that the potential $v_{\mathrm{KS}}[\rho_j]$ exists for each ρ_j. In the case of integer f_i, this silent assumption is known as the condition of "noninteracting v_s-representability" [37]. It means that there exists a Kohn-Sham system for which ρ_j is its ground state. This is an admissibility criterion for ρ_{B} and ρ_{tot} in $v^{\mathrm{NAD}}[\rho_{\mathrm{B}}, \rho_{\mathrm{tot}}]$ [14], namely, there exist Kohn-Sham systems for which each of them is a ground state.

Evaluation of the differences of Kohn-Sham potentials (external, Hartree, and exchange-correlation) is straightforward. The last two terms at the right-hand side of Eq. (5), based on a kinetic-energy functional $T_s[\rho] = -\frac{1}{2}\sum_i f_i\langle\phi_i[\rho]|\nabla^2|\phi_i[\rho]\rangle$, constitute the nonadditive kinetic potential bifunctional $v^{\mathrm{NAD}}[\rho_{\mathrm{B}}, \rho_{\mathrm{tot}}]$. $\phi_i[\rho]$ indicates that the expectation value of the kinetic energy operator is evaluated for optimal orbitals obtained in the constrained search.

The total kinetic energy of a system ($T_s[\rho]$) is the sum over the kinetic energy of all subsystems ($T_s[\rho_j]$) plus an additional "nonadditive" term ($T^{\mathrm{NAD}}[\rho_{\mathrm{A}}, \rho_{\mathrm{B}}]$ in the case of two subsystems), which is due to fermion statistics for electrons and the constrained search definition of the functional $T_s[\rho]$ [38]. The nonadditive kinetic potential bifunctional is defined by the pair of densities provided by total ground-state density $\rho_{\mathrm{tot}}(\mathbf{r})$, and is denoted by $v^{\mathrm{NAD}}[\rho_{\mathrm{B}}, \rho_{\mathrm{tot}}](\mathbf{r})$ where $\rho_{\mathrm{B}}(\mathbf{r})$ is one of the possible partitions of the total density. v^{NAD}, in fact, is the functional derivative of the nonadditive kinetic-energy bifunctional

$$\begin{aligned} v^{\mathrm{NAD}}[\rho_{\mathrm{B}}, \rho_{\mathrm{tot}}](\mathbf{r}) &= \left.\frac{\delta T_s^{\mathrm{NAD}}[\rho, \rho_{\mathrm{tot}}](\mathbf{r})}{\delta\rho(\mathbf{r})}\right|_{\rho=\rho_{\mathrm{B}}} \\ &= \frac{\delta T_s[\rho_{\mathrm{tot}}](\mathbf{r})}{\delta\rho_{\mathrm{tot}}(\mathbf{r})} - \frac{\delta T_s[\rho_{\mathrm{B}}](\mathbf{r})}{\delta\rho_{\mathrm{B}}(\mathbf{r})}, \end{aligned} \tag{6}$$

where ρ_{B} and $\rho_{\mathrm{A}} = \rho_{\mathrm{tot}} - \rho_{\mathrm{B}}$ could be partitioned in different ways, as discussed in Sec. II B. We note that an alternate notation convention is used in other work such as [14], in which the roles of ρ_{A} and ρ_{B} are swapped; i.e., ρ_{A} is the density of the embedded system and $v^{\mathrm{NAD}}[\rho_{\mathrm{A}}, \rho_{\mathrm{tot}}](\mathbf{r})$ is the quantity of interest.

The exact form of $\delta T_s[\rho]/\delta\rho$ is not known (except for the von Weizsäcker formula [36] for the case of one or two electrons, as discussed later), so it needs to be approximated in general. Explicit semi-local approximations to the kinetic-energy functional [18] $T_s[\rho](\mathbf{r})$ in numerical simulations proved useful for applications such as orbital-free DFT [20], but are quite deficient for $v^{\mathrm{NAD}}[\rho_{\mathrm{B}}, \rho_{\mathrm{tot}}]$ [14,24]. Such failures prompted interest in implicit functionals for v^{NAD}, constructed by means of numerical inversion procedures for the Kohn-Sham equation. Unfortunately, this numerical inversion is an

ill-defined problem if finite basis sets are used, which results in numerical instabilities and multiple solutions. While approaches were developed to handle this nonuniqueness [39], the instabilities remain a problem that plagues Kohn-Sham inversion with finite basis sets [40]. Details of the possible inversion procedures and approximations for construction of v^{NAD}, and their difficulties, were reviewed by Banafsheh and Wesolowski, with numerical examples [14]. The Kohn-Sham equations must be inverted twice to obtain $v^{\mathrm{NAD}}[\rho_{\mathrm{B}}, \rho_{\mathrm{tot}}]$ for a given pair of densities, which exacerbates the numerical problems of inversion. Only for some model systems, and particular partitionings of the total density ensuring that $\rho_{\mathrm{tot}} > \rho_{\mathrm{B}}$, can $v^{\mathrm{NAD}}[\rho_{\mathrm{B}}, \rho_{\mathrm{tot}}]$ be expressed analytically [15], and so few results for v^{NAD} from the exact KS potential have been presented in the literature.

A. One-orbital formula

For a Kohn-Sham system described by Eq. (1) with a density as in Eq. (3), we shall consider the special case in which only one orbital is occupied. In this situation, we are able to analytically invert the Kohn-Sham equation [14] and avoid the problems of numerical inversion, a strategy that was employed in many other studies of the exact Kohn-Sham potential [41]. This is the situation for a system of one electron or two spin-compensated electrons.

If this one occupied orbital is real and positive, as is typically the case for the lowest-energy state of a molecule, then $\phi_1(\mathbf{r}) = \sqrt{\rho_1(\mathbf{r})}$. Equation (1) can then be rearranged as:

$$v_{\mathrm{KS}}(\mathbf{r}) = \frac{\nabla^2 \phi_1(\mathbf{r})}{2\phi_1(\mathbf{r})} + \epsilon_1 \tag{7}$$

$$= \frac{\nabla^2 \sqrt{\rho_1(\mathbf{r})}}{2\sqrt{\rho_1(\mathbf{r})}} + \epsilon_1. \tag{8}$$

We define analytical inversion of the density as

$$v^{\mathrm{inv}}[\rho_1](\mathbf{r}) := \frac{\nabla^2 \sqrt{\rho_1(\mathbf{r})}}{2\sqrt{\rho_1(\mathbf{r})}}, \tag{9}$$

which is numerically equivalent to the von Weizsäcker formula, Eq. (16), as discussed below. Here $v^{\mathrm{inv}}[\rho]$ is the effective potential which reproduces the density ρ, which always exists. (By contrast, the effective potential $v_s[\rho]$, for which ρ is the ground state for the noninteracting electron system, exists only if ρ is v_s-representable.) $v^{\mathrm{inv}}[\rho]$ differs from $v_{\mathrm{KS}}[\rho]$, which is an approximate potential using ρ as an ingredient. In the one-orbital formula case

$$v^{\mathrm{inv}}[\rho_1](\mathbf{r}) = v_{\mathrm{KS}}(\mathbf{r}) - \epsilon_1. \tag{10}$$

If we multiply both sides of Eq. (1) by $f_1 \phi_1^*(\mathbf{r})$ we obtain

$$-\tfrac{1}{2}\langle \phi_1 | \nabla^2 | \phi_1 \rangle = \epsilon_1 |\phi_1(\mathbf{r})|^2 - v_{\mathrm{KS}}(\mathbf{r})|\phi_1(\mathbf{r})|^2. \tag{11}$$

Replacing $|\phi_1(\mathbf{r})|^2$ by $\rho(\mathbf{r})$ while identifying the left term in Eq. (11) as $T_s[\rho](\mathbf{r})$, from a functional derivative we obtain

$$v_t[\rho](\mathbf{r}) := \frac{\delta T_s[\rho]}{\delta \rho(\mathbf{r})} = -v_{\mathrm{KS}}[\rho](\mathbf{r}) + \epsilon_1 = -v^{\mathrm{inv}}[\rho](\mathbf{r}). \tag{12}$$

If the exact $T_s[\rho](\mathbf{r})$ is known [in Eq. (6)], then $v^{\mathrm{inv}}[\rho](\mathbf{r}) = -\delta T_s(\mathbf{r})/\delta\rho(\mathbf{r})$.

B. Cusps, singularities, and the nonadditive potential

Let us consider very generally the relationship between cusps in densities and singularities in potentials; we shall define both below. Before beginning, we impose two restrictions on densities and potentials that are assumed throughout the remainder of this work: (1) densities will be obtained from and yield singularity-free Hxc potentials; (2) the states considered always have at least one $1s$ orbital at each nucleus, which dominates the density near each nucleus. Both restrictions apply to the exact ground-state density and potentials. They ensure (see conclusions found in [42]) that cusp conditions [31–33,42,43] hold for cusps in densities and for singularities in both external potentials and approximated Kohn-Sham potentials.

Our goal in this section is to explore how cusps in densities manifest as singularities in nonadditive potentials. Since this varies depending on the nature of densities, we first derive a general rule and then apply it to examples from the literature and to the work done here.

A nuclear cusp means that the angularly averaged density obeys $\lim_{\mathbf{r}\to\mathbf{R}_N} |\nabla\rho| = 2Z_N\rho$; a nuclear singularity means that the potential obeys $\lim_{\mathbf{r}\to\mathbf{R}_N} r_N v \to Z$, where $\mathbf{r}_N = \mathbf{r} - \mathbf{R}_N$. We use a short-hand notation to describe cusps via $e^{-2Z_N|\mathbf{r}-\mathbf{R}_N|}$ and singularities via $-\frac{Z_N}{|\mathbf{r}-\mathbf{R}_N|}$. Each cusp and singularity is uniquely described by $(\mathbf{R}_N, Z_N)$ for nuclei N in some set $N \in \mathcal{N}$. Sums over N without extra clarification imply $N \in \mathcal{N}$.

Note that the notation above addresses behavior near each nucleus, but does not describe every aspect of the system. The true density and potentials may be written as

$$\rho(\mathbf{r}) := \sum_N \rho_{0,N} e^{-2Z_N|\mathbf{r}-\mathbf{R}_N|} + \rho_{\mathrm{smooth}}(\mathbf{r}), \tag{13}$$

$$v(\mathbf{r}) := -\sum_N \frac{Z_N}{|\mathbf{r}-\mathbf{R}_N|} + v_{\mathrm{non\text{-}sing}}(\mathbf{r}), \tag{14}$$

where $\rho_{0,N}$ is the density value at $\mathbf{R}_N$. Here $\rho_{\mathrm{smooth}}(\mathbf{r})$ has no cusps and is zero at each nucleus. $v_{\mathrm{nonsing}}(\mathbf{r})$ has no singularities, but needs few other restrictions. Both functions are discussed in more depth in Appendix A.

All subsequent results follow from three theorems below. The densities involved may be ground-state densities or other densities which have a mapping of the density to the noninteracting potential (Appendix B).

Theorem 1. The density of any electronic system has a cusp of the form $\rho(\mathbf{r}) \approx \rho_{0,N} e^{-2Z_N|\mathbf{r}-\mathbf{R}_N|}$ near every singularity in the external or KS potential, where $v_{\mathrm{ext}}(\mathbf{r}) \approx v_s(\mathbf{r}) \approx -\frac{Z_N}{|\mathbf{r}-\mathbf{R}_N|}$.

Proof. A more general case is a long-known result [31,42]. Here, we use that $\rho_{0,N}$ is nonzero, consistent with our second restriction of having a $1s$ orbital, to narrow it down to systems of relevance. Our first restriction extends it to approximate Kohn-Sham systems. ■

Theorem 2. If the density of an electronic system has a cusp of the form $\rho(\mathbf{r}) \approx \rho_{0,N} e^{-2Z_N|\mathbf{r}-\mathbf{R}_N|}$, then the external and Kohn-Sham potentials have singularities $v_{\mathrm{ext}}(\mathbf{r}) \approx v_s(\mathbf{r}) \approx -\frac{Z_N}{|\mathbf{r}-\mathbf{R}_N|}$.

Proof. The result for interacting systems follows from Theorem 1 and the Hohenberg-Kohn theorem [44,45]. The KS result is easily shown for up to two electrons by using the von

Weizsäcker potential [36]

$$v^{\mathrm{vW}}[\rho](\mathbf{r}) := \frac{\nabla^2\sqrt{\rho(\mathbf{r})}}{2\sqrt{\rho(\mathbf{r})}} \tag{15}$$

$$= \frac{\nabla^2\rho(\mathbf{r})}{4\rho(\mathbf{r})} - \frac{|\nabla\rho(\mathbf{r})|^2}{8\rho^2(\mathbf{r})}, \tag{16}$$

and properties of the Laplacian and gradient. Note that while Eq. (16) is the standard form of v^{vW}, it is analytically equal to the first form in Eq. (15) via the identity

$$\nabla^2\sqrt{\rho(\mathbf{r})} = \frac{2\rho(\mathbf{r})\nabla^2\rho(\mathbf{r}) - [\nabla\rho(\mathbf{r})]^2}{4[\rho(\mathbf{r})]^{3/2}}. \tag{17}$$

Since $v_s(\mathbf{r}) = v^{\mathrm{vW}}[\rho](\mathbf{r}) + C$, for some constant C, the singularities are inherited by v_s. For more than two electrons one may use the results of Appendix B. This extends the known result for exact potentials [42] to well-behaved approximations consistent with our restrictions. ■

Theorem 3. There is thus a one-to-one mapping between cusps in the density and singularities in the external and Kohn-Sham potentials. That is,

$$\rho(\mathbf{r}) \approx \sum_N \rho_{0,N} e^{-2Z_N|\mathbf{r}-\mathbf{R}_N|} \longleftrightarrow -\sum_N \frac{Z_N}{|\mathbf{r}-\mathbf{R}_N|} \approx v \tag{18}$$

up to smooth terms. This includes the important special case of no singularities leading to no cusps, which relies on restriction 1 for approximations to DFT.

Proof. This follows directly from the previous two theorems and a recognition that singularities and cusps near a nucleus at $\mathbf{R}_N$ are smooth functions near a different nucleus at $\mathbf{R}_M \neq \mathbf{R}_N$.

These theorems let us understand how the nonadditive potential in Eq. (6) behaves in the vicinity of a nucleus. We use an alternate form $v_{\mathrm{A,B}}^{\mathrm{NAD}}$ based on ρ_{A} and ρ_{B} here rather than ρ_{B} and ρ_{tot} as in Eq. (6) to define clearly the nature of the total density. The most general result is that the set of singularities in

$$v_{\mathrm{A,B}}^{\mathrm{NAD}}[\rho_{\mathrm{A}}, \rho_{\mathrm{B}}] = v_s[\rho_{\mathrm{B}}] - v_s[\rho_{\mathrm{A}} + \rho_{\mathrm{B}}] \tag{19}$$

[from Eq. (6) and $v_s = -\delta T_s/\delta\rho$] is equal to the set of singularities from ρ_{B} with subtracted the set of singularities from $\rho_{\mathrm{tot}} = \rho_{\mathrm{A}} + \rho_{\mathrm{B}}$, which follows from Theorem 3.

We note that the functional $v_{\mathrm{A,B}}^{\mathrm{NAD}}[\rho_{\mathrm{A}}, \rho_{\mathrm{B}}]$ defined in Eq. (19) resembles the one defined in FDET and analysed in Refs. [27,28] but these functionals have different sets of admissible densities. In FDET, the non-additive kinetic potential is the functional derivative of $T_s^{\mathrm{NAD}}[\rho_{\mathrm{A}}, \rho_{\mathrm{B}}]$ with respect to one of the subsystem densities. For any pair of densities ρ_{tot} and ρ_{B}, which are ground states of Kohn-Sham systems, the potentials given in Eqs. (6) and (19) are well-defined and equal. The necessary condition that this potential is also equal to the functional derivative of $T_s^{\mathrm{NAD}}[\rho_{\mathrm{A}}, \rho_{\mathrm{B}}]$ for a given ρ_{tot} and ρ_{B} is that $T_s^{\mathrm{NAD}}[\rho_{\mathrm{A}}, \rho_{\mathrm{B}}]$ exists for $\rho_{\mathrm{A}} = \rho_{\mathrm{tot}} - \rho_{\mathrm{B}}$. It does not exist, however, if $\rho_{\mathrm{tot}}(r) - \rho_{\mathrm{B}}(r) < 0$ on some measurable volume element.

More precisely, if ρ_{A} has a set of cusps $\mathcal{C}^{\mathrm{A}} := \{(\mathbf{R}_N^{\mathrm{A}}, Z_N^{\mathrm{A}})\}_{N\in\mathcal{N}^{\mathrm{A}}}$, ρ_{B} has a set of cusps $\mathcal{C}^{\mathrm{B}} := \{(\mathbf{R}_N^{\mathrm{B}}, Z_N^{\mathrm{B}})\}_{N\in\mathcal{N}^{\mathrm{B}}}$, and $\rho_{\mathrm{tot}} = \rho_{\mathrm{A}} + \rho_{\mathrm{B}}$ has a set of cusps $\mathcal{C} := \{(\mathbf{R}_N, Z_N)\}_{N\in\mathcal{N}}$, then the singular part of the nonadditive potential in Eq. (19) is

$$v_{\mathrm{sing}}^{\mathrm{NAD}}(\mathbf{r}) = \sum_{N\in\mathcal{N}^{\mathrm{B}}} \frac{-Z_N^{\mathrm{B}}}{|\mathbf{r}-\mathbf{R}_N^{\mathrm{B}}|} + \sum_{N\in\mathcal{N}} \frac{Z_N}{|\mathbf{r}-\mathbf{R}_N|}. \tag{20}$$

Although we treated $\mathcal{C}$ as independent above, it follows from $\rho_{\mathrm{tot}} = \rho_{\mathrm{A}} + \rho_{\mathrm{B}}$ that $\mathcal{C}$ can be obtained from $\mathcal{C}^{\mathrm{A}}$ and $\mathcal{C}^{\mathrm{B}}$ by the following rules: (i) if $\mathbf{R} = \mathbf{R}_N^{\mathrm{A}} = \mathbf{R}_M^{\mathrm{B}}$ for some $N \in \mathcal{N}^{\mathrm{A}}$ and $M \in \mathcal{N}^{\mathrm{B}}$ then $\mathcal{C}$ has a combined cusp $(\mathbf{R}, \frac{\rho_{\mathrm{A}}(\mathbf{R})Z_N^{\mathrm{A}} + \rho_{\mathrm{B}}(\mathbf{R})Z_M^{\mathrm{B}}}{\rho_{\mathrm{tot}}(\mathbf{R})})$; (ii) other cusps in A and B are included unmodified. Either set can be empty (although this would be very strange for $\mathcal{C}$), leading to zero for the corresponding sum.

Applying these rules depends on precise details of the embedding or partitioning scheme. The next sections therefore apply Eq. (20) to the case of smooth partitioning of densities studied here, as well as to some cases from the literature.

1. Smooth partitioning of densities

The remainder of the article deals with densities that are partitioned according to $\rho_{\mathrm{A}}(\mathbf{r}) = w(\mathbf{r})\rho_{\mathrm{tot}}(\mathbf{r})$ and $\rho_{\mathrm{B}} = [1 - w(\mathbf{r})]\rho_{\mathrm{tot}}(\mathbf{r})$ where $0 < w(\mathbf{r}) < 1$ is a smooth, cusp-free, and positive function. $1 - w$ therefore has the same qualities as w. In this case, the nonadditive potential has no cusps.

To show this, we recognize that ρ_{A}, ρ_{B}, and ρ_{tot} *all* have the same cusps, which follows from the definition of the density and from w and $1 - w$ being smooth and finite, so that they only contribute to smooth terms. Therefore, $\mathcal{C}^{\mathrm{A}} = \mathcal{C}^{\mathrm{B}} = \mathcal{C}$ and we obtain

$$v_{\mathrm{sing}}^{\mathrm{NAD,part}}(\mathbf{r}) = 0. \tag{21}$$

In Sec. III, we numerically apply a smooth cusp-less function to partition the ground-state density of some model diatomic systems of two and four electrons and we show that the corresponding nonadditive potential indeed has no singularities at the nuclei, consistent with theory.

2. Embedding with a cusp-free density ρ_{B}

In some cases, one obtains a density ρ_{B} that is cusp-free in some region of interest, but otherwise has the same cusps as ρ_{tot}, as implicitly assumed in Appendix A of García-Lastra *et al.* [27]. This situation happens for, e.g., embedding calculations where some molecules (with cusps at nuclei) are treated at one level of theory and an additional molecule (with existing cusps and new cusps at the additional nuclei) is embedded in the precomputed set. This is the typical setup for FDET combining different levels of electronic structure theory [1]. Such situations can also arise via a nonsmooth partitioning in which $w(\mathbf{r})$ has a constant value of 0 in some region. In such a case, the difference between effective potentials $v_s[\rho_{\mathrm{tot}}]$ and $v_s[\rho_{\mathrm{B}}]$ is not uniquely defined [46].

As a result, all cusps of ρ_{B} appear in ρ_{A} and ρ_{tot}, but not vice versa. All cusps appear with the same value and at the same nuclear positions when they are present, giving $\mathcal{C}^{\mathrm{A}} = \mathcal{C}$. We use $\mathcal{N}_{\mathrm{A}\notin\mathrm{B}}$ to denote nuclei yielding cusps in A and $A + B$ that are not in B. It follows that

$$v_{\mathrm{sing}}^{\mathrm{NAD,emb}}(\mathbf{r}) = \sum_{N\in\mathcal{N}_{\mathrm{A}\notin\mathrm{B}}} \frac{Z_N}{|\mathbf{r}-\mathbf{R}_N|}. \tag{22}$$

In accordance with this analysis, a nuclear singularity was found in Appendix A of [27]. This situation also arises when the density is partitioned not in space but by orbital, so that ρ_A, ρ_B, and ρ_{tot} all have the same cusps. An exactly solvable atom-like model system was studied in this way in [15] and a nuclear singularity was also found, as expected from our reasoning.

3. Use of a finite basis to represent densities

Another interesting case is one where densities are obtained using a finite basis set. We first consider a Slater-type orbital (STO) basis set, which is able to reproduce cusps, but where the resulting cusps are imperfect [24]. In a finite STO basis one obtains $\rho(\mathbf{r}\to\mathbf{R}_N)\approx\rho(\mathbf{R}_N)e^{-\tilde{Z}_N|\mathbf{r}-\mathbf{R}_N|}$ where $\tilde{Z}_N$ is the finite basis approximation for Z_N. $\tilde{Z}_N\approx Z_N$ varies with choice of basis, choice of density functional approximation, and other details of the calculation.

For convenience we assume that all densities contain all cusps, as in Sec. II B 1. This leads to ρ_A, ρ_B, and ρ_{tot} defined by cusp sets $\mathcal{C}^A=\{(\tilde{Z}_N^A,\mathbf{R}_N)\}$, $\mathcal{C}^B=\{(\tilde{Z}_N^B,\mathbf{R}_N)\}$, and $\mathcal{C}=\{(\tilde{Z}_N,\mathbf{R}_N)\}$, respectively. Importantly, $\mathbf{R}_N$ is the same in all cases but $\tilde{Z}_N^A\approx\tilde{Z}_N^B\approx\tilde{Z}_N$ are not the same (but are similar) because of errors introduced by the finite basis. The singular part of the nonadditive potential is therefore

$$v_{\text{sing}}^{\text{NAD,STO}}=\sum_{N\in\mathcal{N}}\frac{\tilde{Z}_N-\tilde{Z}_N^B}{|\mathbf{r}-\mathbf{R}_N|},\tag{23}$$

where the terms $\tilde{Z}_N-\tilde{Z}_N^B$ in the numerator are effectively random artifacts, defined by the basis set and other computational and methodological choices. These artifacts also apply to embedding, per Sec. II B 2. Equation (23) then acts in addition to the "exact" cusps from Eq. (22).

Gaussian-type orbitals (GTOs), used in many quantum chemistry calculations, cannot reproduce cusps at all, unlike STOs, as they are analytic near nuclei. Nevertheless, they have an effective analogue to Eq. (23) for small but finite r_N in the vicinity of a nucleus.

Of greatest relevance to the present work is that calculations on a finite grid (adapted to the description of nuclear cusps and singularities, as discussed in Sec. III) can eliminate these errors entirely. This involves the effective use of numerical methods, chosen such that the derived potentials are as consistent as possible with the routines used to solve the effective Hamiltonians. Specifically, one should use $\frac{\nabla^2\sqrt{\rho}}{2\sqrt{\rho}}$ [Eq. (16)] rather than the mathematically equivalent $\frac{\nabla^2\rho}{4\rho}-\frac{|\nabla\rho|^2}{8\rho^2}$ [Eq. (16)] when computing potentials.

III. NUMERICAL CALCULATIONS

To confirm the validity of the analyses above in a case of the smooth partitioning of densities, we perform numerical calculations with the all-electron DFT package DARSEC [47], which is designed for high-precision calculations on diatomic molecules, including Kohn-Sham inversions [48]. In DARSEC, the Kohn-Sham equations are solved self-consistently using a high-order finite difference approach [49,50]. A real-space grid based on prolate-spherical coordinates is used to describe a system with two atomic centers. The grid is dense near the atoms and increasingly sparse farther away. This atom-adapted grid provides precise information at the vicinity of the nuclei to enable exploration of the density and potential at these points. It also enables treatment of the singular Coulomb potential at the nuclei, unlike the usual Cartesian grids used in real-space codes, which are not designed for all-electron calculations [51]. Due to the cylindrical symmetry of diatomic molecules, the three-dimensional problem is reduced to a two-dimensional one in DARSEC. In this work, the systems are defined within an ellipse with semiminor radius of 15 bohr and use a 115×121 set of grid points for coordinates μ and ν. DFT calculations were performed using the local density approximation (LDA) [52,53].

We carefully examined the numerical precision of our calculations, given the difficulty of describing cusps and singularities numerically, and the possibility of numerical artifacts being mistaken for cusps or singularities. We find robust results in our tests on stencil size and dividing by denominators close to zero [54]. Tests show a high degree of mirror symmetry within the region of interest $z\in[-4,+4]$ bohr in $v^{\text{NAD}}[\rho_B,\rho_{tot}](\mathbf{r})$ or $v^{\text{NAD}}[\rho_A,\rho_{tot}](\mathbf{r})$ for homonuclear diatomic systems, which is enabled by the symmetry of our weighting function. As seen below, nuclear cusps for the density and singularities for v_{KS} are well reproduced. The only hint of a singularity in v^{NAD} comes from using a clearly inadequate stencil size of 2 or an extremely sharp cutoff in $w(\mathbf{r})$ for partitioning, clearly numerical in both cases [54]. For all calculations in this article, the finite-difference stencil size was set to 12, as per standard recommendations for DARSEC. We additionally demonstrate below excellent agreement between analytically inverted $v^{\text{inv}}[\rho]$ and $v^{\text{KS}}[\rho]$, and between $v^{\text{NAD}}[\rho_B,\rho_{tot}]$ from analytical inversion and from the von Weizsäcker potential.

Based on Eq.(9), we implement in our modified version of DARSEC the equation

$$v^{\text{NAD/INV}}[\rho_B,\rho_{tot}](\mathbf{r})=v^{\text{inv}}[\rho_B](\mathbf{r})-v^{\text{inv}}[\rho_1](\mathbf{r}),\tag{24}$$

where $\rho_1(\mathbf{r})=2|\phi_1(\mathbf{r})|^2$ and $\phi_1(\mathbf{r})$ is the lowest-energy orbital. This analytical inversion is appropriate when the conditions for the one-orbital formula are satisfied (Sec. II A).

A. Von Weizsäcker potential

Because the von Weizsäcker potential v^{vW} is mathematically equivalent to v^{inv} for densities based on one orbital, we can also obtain correct results for v^{NAD} when using v^{vW} in place of v^{inv} for calculating subsystems of either one or two electrons, as follows

$$v^{\text{NAD/vW}}[\rho_B,\rho_{tot}](\mathbf{r})=v^{\text{vW}}[\rho_B](\mathbf{r})-v^{\text{vW}}[\rho_1](\mathbf{r}),\tag{25}$$

using $v^{\text{vW}}[\rho(\mathbf{r})]$ as given in Eq. (16). While, as argued in Sec. II B 3, such results are expected to give less precise results than the approach with Eq. (15) [namely $v^{\text{NAD/INV}}$, Eq. (24)], we demonstrate good agreement between the two formulations which proves the numerical precision of our calculations. It is important to note the difference between this equation and Eq. (6): the second term uses ρ_1 not ρ_{tot}, as we would have if we were to take von Weizsäcker as simply an approximation to $\delta T_s/\delta\rho$, as was considered in [14]. Such a formula would be exact only when both ρ_B and ρ_{tot} are one

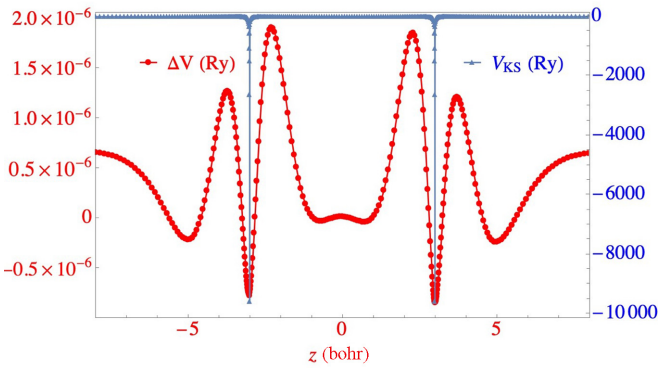

FIG. 1. Difference between the analytically inverted $v^{\text{inv}}[\rho_1](\mathbf{r})$ and $v^{\text{KS}}(\mathbf{r})$ for HeHe, showing agreement to 1 part in 10^{10}. Blue: $v^{\text{KS}}(\mathbf{r})$. Red: $\Delta v = v^{\text{KS}}(\mathbf{r}) - v^{\text{inv}}[\rho_1](\mathbf{r})$.

or two electrons, i.e., in the case of H_2 but not of HeHe or $HeLi^+$. However, by using instead a two-electron density from the orbital ϕ_1 we can have a correct formula also for HeHe and $HeLi^+$. Such a formula is equivalent, up to a constant, to using v_{KS} instead of $v^{\text{vW}}[\rho_1]$; we tested this option as well and found very close agreement, consistently with Fig. 1 below.

We compare our v^{NAD} with $v^{\text{NAD/vW}}$ as a benchmark to help examine whether there are any artifacts due to numerical differences from evaluation using the Laplacian or the gradient. In Sec. IV, we show the very close agreement of $v^{\text{NAD/vW}}$ and v^{NAD} for our three test systems, demonstrating the numerical precision of our calculations.

B. Localization of one or two electrons

For partitioning the ground-state density numerically, we use a smooth distribution function $0 \leqslant F(z) \leqslant 1$ that has no cusps and respects the smoothness of the function explained in Sec. II B 1. Specifically, we use the Fermi-Dirac distribution function

$$F(z - z_0) = \frac{1}{e^{\alpha(z-z_0)} + 1}, \tag{26}$$

where z_0 is the cutoff that sets the z at which $F = 0.5$, and α is the curve-smoothing parameter. Other similar sigmoid functions could also be used for this purpose. By partitioning the total density of the diatomic system aligned along the z axis into two subdensities we obtain $\rho_{\text{B}}(\mathbf{r}) = F(z - z_0)\rho_{\text{tot}}(\mathbf{r})$ and $\rho_{\text{A}}(\mathbf{r}) = \rho_{\text{tot}}(\mathbf{r}) - \rho_{\text{B}}(\mathbf{r})$.

In a diatomic system of $N = 2 + 2M$ (for integer M) electrons where two spin-compensated electrons can be localized around one nucleus, we choose z_0 to satisfy the following condition:

$$\int \rho_{\text{B}}(\mathbf{r})d\mathbf{r} = \int F(z - z_0)\rho_{\text{tot}}(\mathbf{r})d\mathbf{r} = 2. \tag{27}$$

For the case of one-electron localization, z_0 can be chosen so that the integral of Eq. (27) is instead 1. We find z_0 via a binary-search algorithm, with tolerance 10^{-15} for the difference of the integral from 2 (or 1). For homonuclear systems, z_0 should be exactly zero by symmetry. We quantify the density overlap in these systems as

$$\int \rho_{\text{A}}(\mathbf{r})\rho_{\text{B}}(\mathbf{r})d\mathbf{r}. \tag{28}$$

TABLE I. Summary of key properties for diatomic systems used in this work. The density overlap is defined in Eq. (28).

System	N_e total	N_e in ρ_{B}	Cutoff z_0 (bohr)	Density overlap (e^2/bohr^3)
HeHe	4	2	0	3.81×10^{-6}
$HeLi^+$	4	2	−0.29	2.51×10^{-3}
H_2	2	1	0	1.75×10^{-5}

In the present calculations $\alpha = 20$ bohr^{-1} was chosen after testing different values [54]. Too small a value does not constitute localization on one nucleus and too large a value (for a given grid) leads to numerical discontinuities and artifacts at z_0. Unlike the grid spacing, α is not a numerical parameter to be converged, but rather defines the way which we choose to partition the density. The main effect of changing α within a range 15–50 bohr^{-1} is that the plateau of v^{NAD} becomes narrower and taller with larger α (a smaller transition region between 0 and 1). This behavior gives an indication of how the width of the transition in other sigmoidal functions would affect v^{NAD}. Such effects are simply a feature that must be taken into account consistently with the density partitioned using a given partitioning function.

IV. RESULTS AND DISCUSSION

Two classes of diatomic model systems were chosen for this study. One class contains two electrons in total and one electron was localized around one nucleus; we use the homonuclear H_2. In the second class, there are four electrons in total and two electrons were localized around one nucleus; we use the homonuclear HeHe and the heteronuclear $HeLi^+$. Key properties of these systems for our studies are summarized in Table I. For each system, we compare the analytically inverted potential with $v^{\text{NAD/vW}}$ from Eq. (25).

We study systems with weakly overlapping subsystem densities, in part to enable direct comparison with [14], in which singularities were previously reported in v^{NAD}. All calculations are done for a stretched interatomic distance of 6 bohr, centered on $z = 0$. For homonuclear systems, the maximum density overlap between the subdensities occurs at $z = 0$ by symmetry, while for the heteronuclear systems the location of maximum overlap occurs closer to the nucleus with smaller atomic number.

The graphical representations of the results are provided in one and two dimensions. The one-dimensional (1D) plot is the contour along the minimum value of μ used, which is closest to the interatomic z axis since there are no grid points at $x = 0, y = 0$.

A. Two-electron localization

1. Homonuclear model system: HeHe

We begin the study of this system by demonstrating the numerical precision of our analytical inversion from Eq. (8)

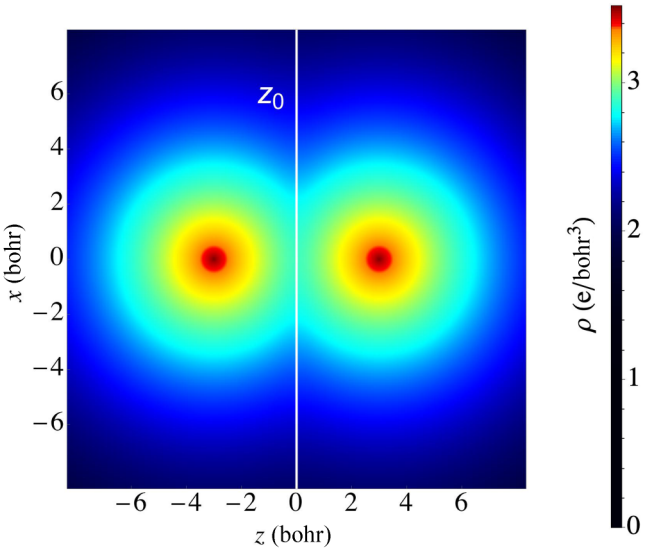

FIG. 2. Ground-state charge density distribution of HeHe in two dimensions. The vertical line indicates the cutoff plane where $z = z_0$, dividing the two localized densities which integrate to two electrons.

for $\rho_1 = 2|\phi_1(\mathbf{r})|^2$ and for the eigenvalue ϵ_1 by comparing to the Kohn-Sham potential from the SCF calculation. We find that indeed $\Delta v = v_{\rm KS} - v^{\rm inv}[\rho_1] \approx 0$, as shown in Fig. 1. The difference between the two is approximately ten orders of magnitude less than the values of the potential, showing excellent precision. The reduction of precision by the square root function is the main contributor to the residual difference. Δv is smooth and in particular well behaved around the nuclei. The singularities at the nuclei are well reproduced for $v_{\rm KS}$, as per Eq. (14).

The charge density for HeHe including its partitioning is depicted in two dimensions in Fig. 2. The nuclear cusps are clearly seen, as in Eq. (13). The system is symmetrical about the $z = 0$ plane, and therefore the cutoff z_0 from Eq. (26) is exactly at $z = 0$. Consequently, $\rho_{\rm A}$ and $\rho_{\rm B}$ both integrate to 2, each localized around a different nucleus with close to zero charge density in the vicinity of the opposite nucleus, as shown in one dimension in Fig. 3(a).

We now proceed to analyze $v^{\rm NAD}$, as shown in one dimension in comparison to the input densities in Fig. 3. For $\rho_{\rm B}$ localized on the left, we see a shape which starts with a small positive value and has a small attractive well at the overlap region of $z = 0$, a barrier, and another small attractive well at the right nucleus. This surprising attractive well at the other nucleus can be attributed to the feature discussed in Sec. II B 1, in which $\rho_{\rm B}$ must have a cusp at both nuclei; the well induces the extra density for the cusp at the other nucleus. There is a wall at the location of the right nucleus with a plateau afterward, preventing $\rho_{\rm B}$ from entering that region. The wall and plateau are similar to the results found with finite basis sets [24], though in that case the wall was not exactly at the nucleus but displaced slightly in the direction of the other nucleus. While the wall is a sharp feature, it is smooth with several points along it, and there is no sign of any cusps or singularities. We compare $v^{\rm NAD/INV}$ to $v^{\rm NAD/vW}$ in Fig. 3(b) and find excellent agreement with differences around 1 part in

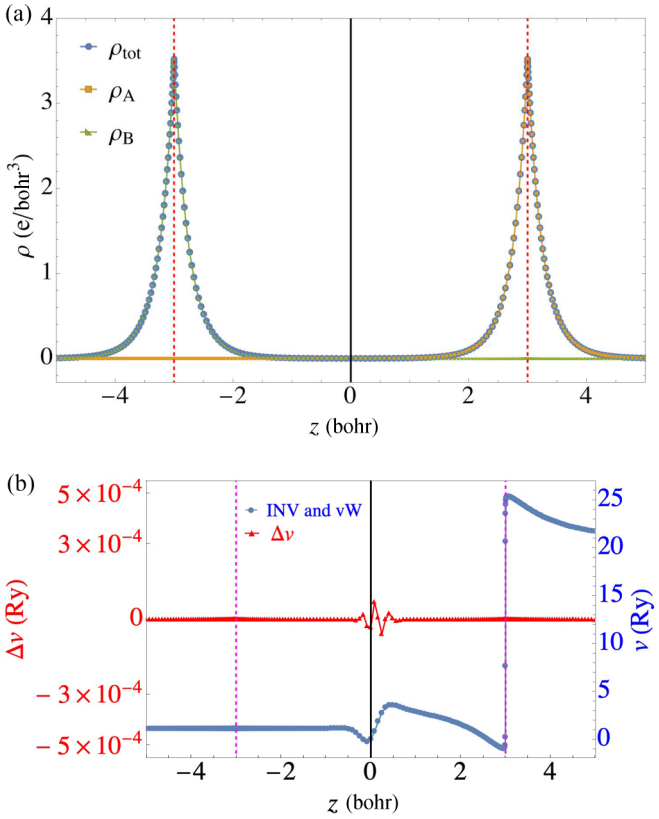

FIG. 3. Nonadditive kinetic potential for HeHe, in a 1D representation. Purple dashed lines mark the location of the nuclei and a black solid line marks the cutoff z_0. (a) Total and partitioned densities. (b) Analytically inverted kinetic potential $v^{\rm NAD/INV}[\rho_{\rm B}, \rho_{\rm tot}](\mathbf{r})$ [from Eq. (24)], where the localized density $\rho_{\rm B}$ is on the left, compared to the same from von Weizsäcker theory [from Eq. (25)]. Blue: $v^{\rm NAD/INV}$; Red curve: $\Delta v = v^{\rm NAD/vW} - v^{\rm NAD/INV}$.

10^5, found mainly in the overlap region, where the division by small ρ is most ill-conditioned.

We further examine $v^{\rm NAD}$ in the two-dimensional (2D) representation to see the behavior away from the z axis (Fig. 4). We see that $v^{\rm NAD}$ is essentially constant in the $z < 0$ region. The well around $z = 0$ becomes increasingly attractive away from the z axis, but the well at the right nucleus is located only near the z axis. The plateau falls away slowly from the z axis. The steep wall at the right nucleus can be clearly seen, but no cusps or singularities are visible here either. We again compare $v^{\rm NAD/INV}$ and $v^{\rm NAD/vW}$, now in two dimensions, and see no perceptible difference except small deviations around $x = 6$ bohr near the cutoff, where the density is very small (Fig. 4).

2. *Heteronuclear model system:* HeLi$^+$

Next we consider a heteronuclear system, again with four electrons: HeLi$^+$. We localize two electrons on the Li atom side, which has $z < 0$ and is on the left in our plots. We find a cutoff $z_0 = -0.29$ bohr, which is slightly closer to the nucleus with the larger atomic number since it has a more steeply decaying density according to Eq. (13) [Fig. 5(a)]. The density overlap is larger than for HeHe (Table I).

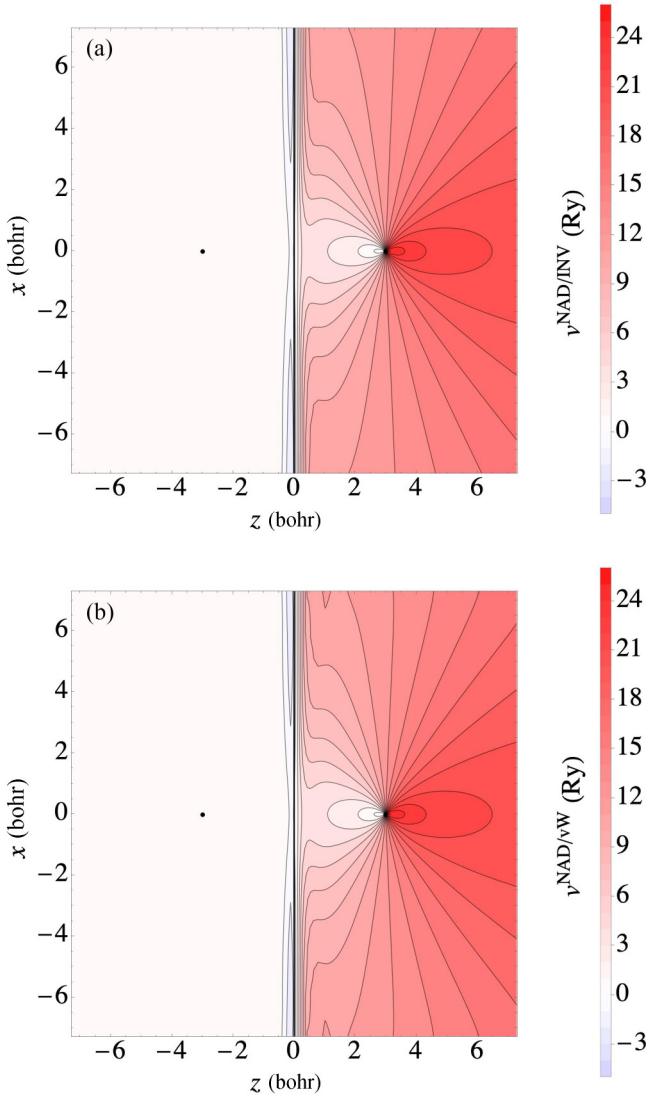

FIG. 4. Nonadditive kinetic potential for HeHe in a 2D representation, comparing (a) $v^{\mathrm{NAD/INV}}$ with (b) $v^{\mathrm{NAD/vW}}$, both in Ry. The density is localized on the left nucleus. Black dots mark the nuclei and a black line marks the cutoff z_0.

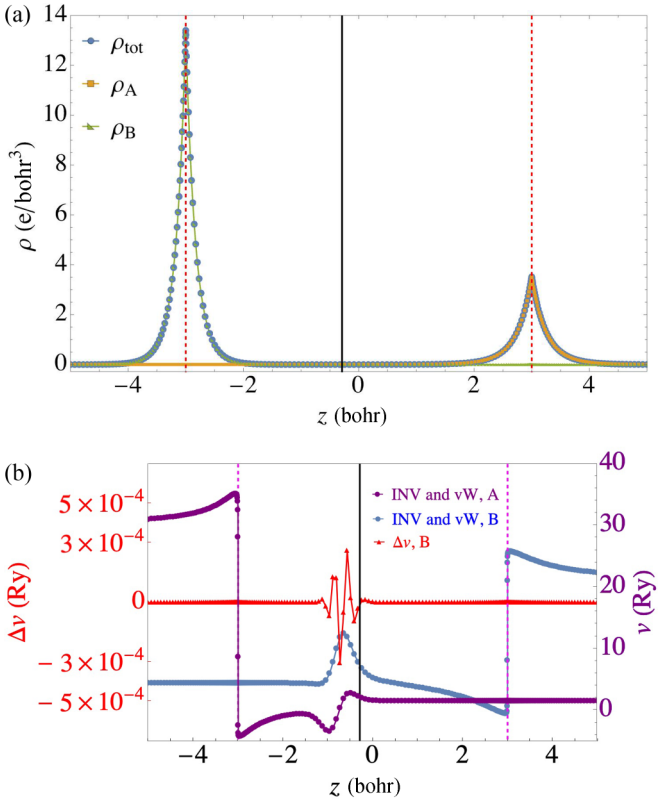

FIG. 5. Nonadditive kinetic potential for $HeLi^+$ (with Li on the left side), in a 1D representation. Purple dashed lines mark the location of the nuclei and a black solid line marks the cutoff z_0. (a) Total and partitioned densities, with a taller peak for Li. (b) Analytically inverted kinetic potential $v^{\mathrm{NAD/INV}}[\rho_B, \rho_{tot}](\mathbf{r})$ [from Eq. (24)], which is localized on the Li side (blue), compared to the same from von Weizsäcker theory [from Eq. (25)], with $\Delta v = v^{\mathrm{NAD/vW}} - v^{\mathrm{NAD/INV}}$ in red. Also shown is $v^{\mathrm{NAD/INV}}[\rho_A, \rho_{tot}](\mathbf{r})$ which is localized on the He side (purple).

In this case, we can actually calculate two distinct quantities, $v^{\mathrm{NAD/INV}}[\rho_B, \rho_{tot}](\mathbf{r})$ (localized on Li) and $v^{\mathrm{NAD/INV}}[\rho_A, \rho_{tot}](\mathbf{r})$ (localized on He), as shown in Fig. 5(b). For HeHe, the corresponding quantities are identical by symmetry. The shape and magnitude of $v^{\mathrm{NAD}}[\rho_B, \rho_{tot}](\mathbf{r})$ is similar to that of HeHe, with a small positive value on the left and a wall and plateau on the right. In the overlap region, however, there is not a step but rather a small peak just to the left of z_0, and then a small slightly attractive well just on the left side of the He nucleus, next to the steep wall. This well again can be related to the need to induce a cusp. $v^{\mathrm{NAD}}[\rho_A, \rho_{tot}](\mathbf{r})$ has a similar shape, albeit flipped horizontally, and with a smaller peak, two attractive wells, and a higher wall. The fact that there are two attractive wells is in common with He localized in HeHe.

We compare $v^{\mathrm{NAD/INV}}[\rho_B, \rho_{tot}](\mathbf{r})$ and $v^{\mathrm{NAD/vW}}[\rho_B, \rho_{tot}](\mathbf{r})$ and find again excellent agreement with differences Δv around 1 part in 10^4, largest around the peak next to the overlap region. The 2D plots in Fig. 6 also show no perceptible difference between $v^{\mathrm{NAD/INV}}$ and $v^{\mathrm{NAD/vW}}$, except small deviations around $x = 6$ bohr near the cutoff. The shapes are similar to HeHe, except that v^{NAD} is not constant on the left and decreases away from the z axis. The positive peak just to the left of $z = 0$ becomes an attractive well like HeHe, centered about 5 bohr from the z axis. No cusps or singularities are seen in the 1D or 2D plots.

B. One-electron localization for H_2

Our third test system is the stretched H_2 system in which one electron is localized around the left nucleus. The cutoff is $z_0 = 0$ by symmetry. The v^{NAD} (Fig. 7) shows magnitude and features similar to those of HeHe and $HeLi^+$. There is a small attractive well at the overlap region and then a step and a small well at 5 Ry just to the left of the right nucleus. $v^{\mathrm{NAD/vW}}$ and $v^{\mathrm{NAD/INV}}$ agree well with differences again mainly in the overlap region. The 2D view of v^{NAD} (Fig. 8) is very similar to HeHe, but with little variation in the attractive well away from the z axis. The only differences between $v^{\mathrm{NAD/INV}}$ and $v^{\mathrm{NAD/vW}}$ are small deviations in $x > 4$ bohr, in a larger region

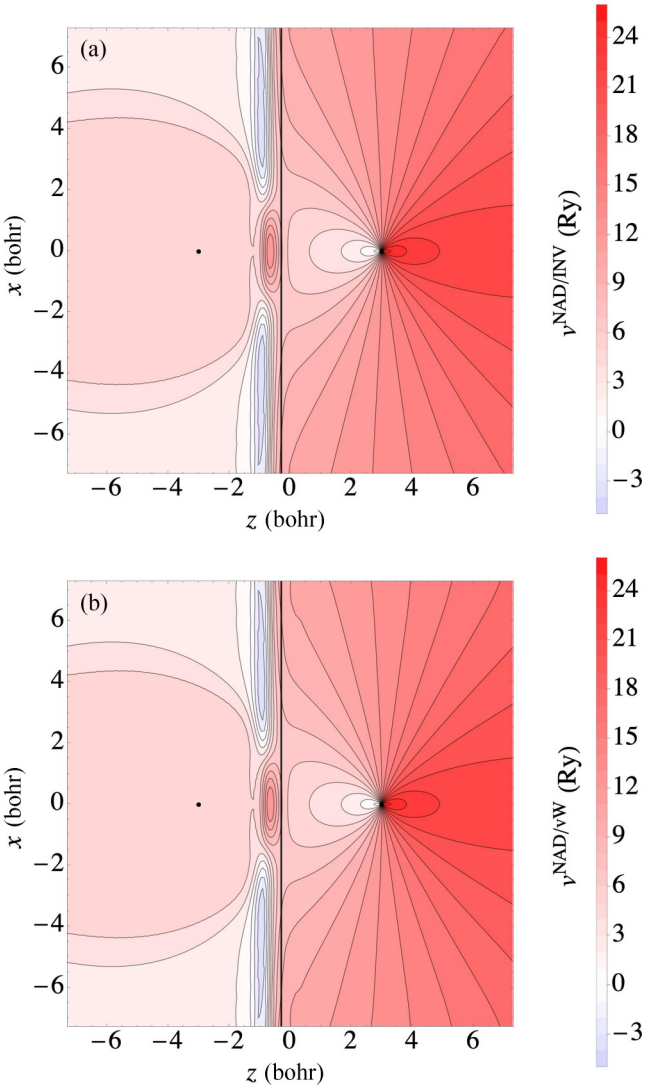

FIG. 6. Nonadditive kinetic potential for $HeLi^+$ in a 2D representation, comparing (a) $v^{NAD/INV}[\rho_B, \rho_{tot}](\mathbf{r})$ with (b) $v^{NAD/vW}[\rho_B, \rho_{tot}](\mathbf{r})$, both in Ry. The density is localized on Li, on the left. Black dots mark the nuclei and a black line marks the cutoff z_0.

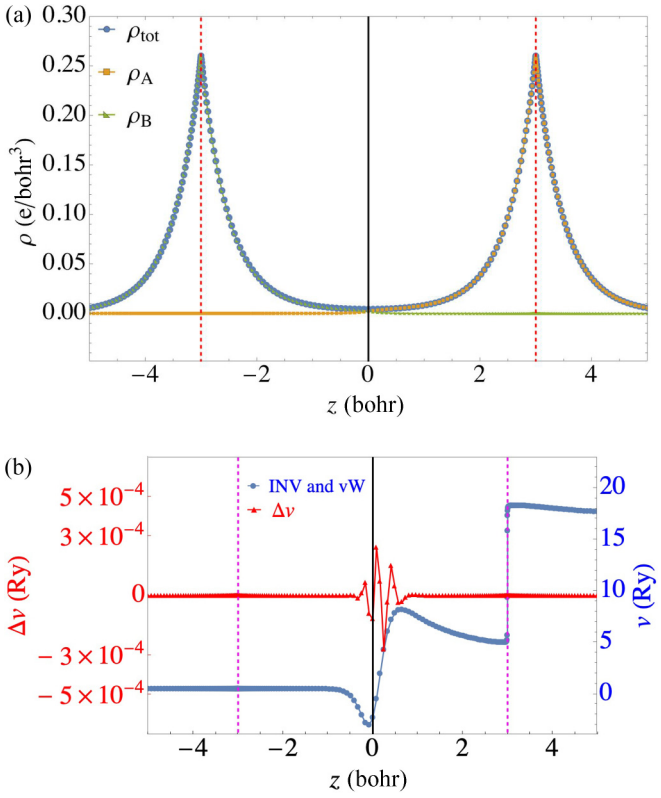

FIG. 7. Nonadditive kinetic potential for H_2, in a 1D representation, where one electron is localized. Purple dashed lines mark the location of the nuclei and a black solid line marks the cutoff z_0. (a) Total and partitioned densities. (b) Analytically inverted kinetic potential $v^{NAD/INV}[\rho_B, \rho_{tot}](\mathbf{r})$ [from Eq. (24)], where the localized density ρ_B is on the left, compared to the same from von Weizsäcker theory [from Eq. (25)]. Blue: $v^{NAD/INV}$; Red curve: $\Delta v = v^{NAD/vW} - v^{NAD/INV}$.

than for HeHe or $HeLi^+$. No cusps or singularities are seen in the 1D or 2D plots.

V. CONCLUSION

In this work, we investigated analytically and numerically the presence of singularities in the nonadditive kinetic potential v^{NAD} and resolved the uncertainty that surrounded this question, for a variety of important cases of relevance to partitioning schemes. For two partitioned subdensities that overlap smoothly and have cusps at all nuclei (Sec. II B 1), the inverted potential of each has singularities at the vicinity of both nuclei, which then cancel. $v^{NAD}[\rho_B, \rho_{tot}](\mathbf{r})$ has no singularities at the nuclei and must be smooth everywhere. This situation is convenient for approximations since the singularities are difficult to capture and a smooth v^{NAD} is easier to use in practical calculations. By contrast, in the usual embedding-theory situation where the subdensity is zero at some nuclei and lacks cusps there (Sec. II B 2), there are singularities in v^{NAD}. Singularities can also arise due to the use of Slater-type orbitals or other basis sets that do not perfectly describe cusps (Sec. II B 3). Our analysis applies to both the exact KS potential under some physically likely assumptions and to all approximated forms known to the authors.

We confirmed these analytic results and demonstrate that they are achievable numerically with the LDA by performing grid-based all-electron calculations for diatomic systems HeHe, $HeLi^+$, and H_2, and by computing $v^{NAD}[\rho_B, \rho_{tot}]$ from analytic inversion. The examination of $v^{NAD}[\rho_B, \rho_{tot}]$ in one and two dimensions demonstrated smooth behavior and no cusps or singularities, unlike in [14]. We established that the analytically inverted v^{inv} from an orbital and eigenvalue agrees closely with the Kohn-Sham potential used to evaluate the density. We showed a way of calculating $v^{NAD}[\rho_B, \rho_{tot}]$ exactly using the von Weizsäcker potential for these systems since it is exact for one orbital. We benchmarked our calculations from analytic inversion against $v^{NAD/vW}[\rho_B, \rho_{tot}]$ and confirmed the close equality of these potentials throughout space for all three diatomic systems, ensuring that the analytically inverted potential is numerically precise and does not suffer from numerical artifacts.

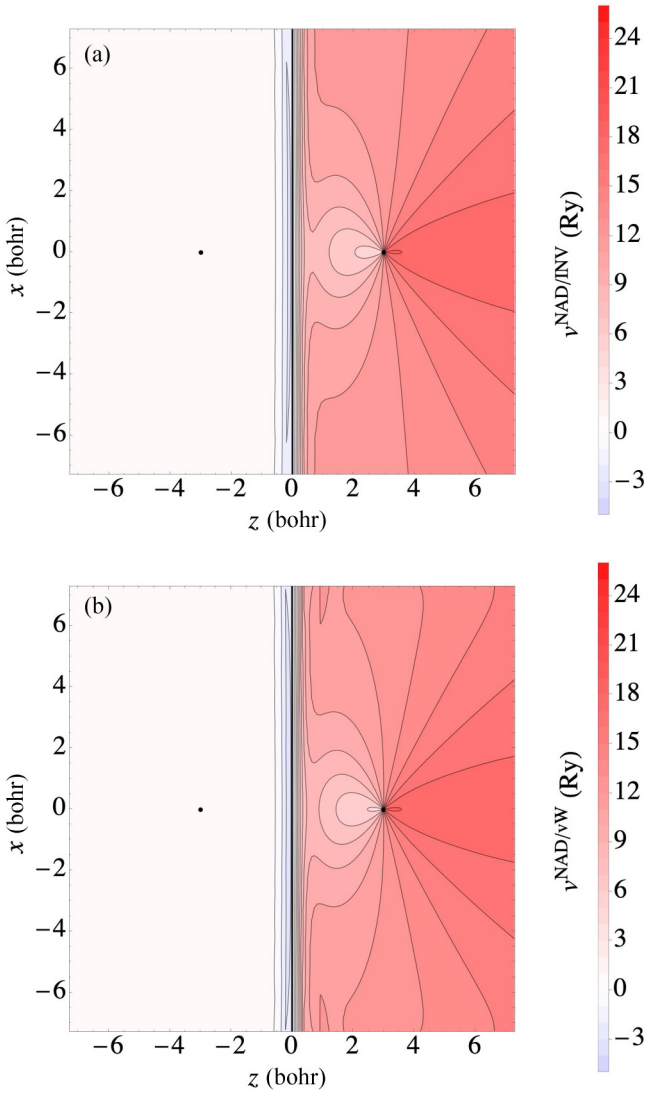

FIG. 8. Nonadditive kinetic potential for H_2 in a 2D representation, comparing (a) $v^{\mathrm{NAD/INV}}$ with (b) $v^{\mathrm{NAD/vW}}$, both in Ry. Black dots mark the nuclei and a black line marks the cutoff z_0.

Using our reliable results for $v^{\mathrm{NAD}}[\rho_{\mathrm{B}}, \rho_{\mathrm{tot}}]$, we were able to learn about its exact features (for LDA). The potentials shown in Figs. 3, 5, and 7(b) feature a step and a barrier between the two nuclei. These are desired and expected features of $v^{\mathrm{NAD}}[\rho_{\mathrm{B}}, \rho_{\mathrm{tot}}](\mathbf{r})$ evaluated for a pair of densities $\rho_{\mathrm{B}}(\mathbf{r})$ and $\rho_{\mathrm{tot}}(\mathbf{r})$ for which $\rho_{\mathrm{tot}} - \rho_{\mathrm{B}}$ disappears near the nucleus B. From a practical perspective, any approximation to v^{NAD} should reproduce these features. Practical calculations using an approximated v^{NAD} that do not reproduce these features are prone to an artificial leak of electrons onto the nucleus B (for a detailed discussion of this issue see [27]).

This work demonstrates the exact features of v^{NAD} which can be used to develop and test numerical inversion schemes, kinetic-energy functionals, or nondecomposable approximations that target v^{NAD} directly. The analytic inversion approach can be used for further exploration of exact properties of v^{NAD} in other systems.

ACKNOWLEDGMENTS

We thank Dr. Rachel Garrick for help with development in DARSEC and Elsa Vazquez for help in preparing plots. M.B. and D.S. were supported as part of the Consortium for High Energy Density Science by the U.S. Department of Energy, National Nuclear Security Administration, Minority Serving Institution Partnership Program, under Awards No. DE-NA0003866 and No. DE-NA0003984, and by UC Merced start-up funds. T.G. was supported by Australian Research Council Grants No. DP200100033 and No. FT210100663. L.K. thanks the Aryeh and Mintzi Katzman Professorial Chair and the Helen and Martin Kimmel Award for Innovative Investigation. Computational resources were provided by the Multi-Environment Computer for Exploration and Discovery (MERCED) cluster at UC Merced, funded by National Science Foundation Grant No. ACI-1429783.

APPENDIX A: SMOOTH DENSITIES, CUSPS, AND NONSINGULAR POTENTIALS

Densities of electronic systems are finite, meaning that at any point $\mathbf{R}_N$ we can make a series expansion in small $\mathbf{r}_N = \mathbf{r} - \mathbf{R}_N$. The general formula for expansion of ρ is,

$$\rho(\mathbf{r}) = \rho_{0,N} + b_\rho r_N + \boldsymbol{B}_\rho \cdot \mathbf{r}_N + r_N \boldsymbol{C}'_\rho \cdot \mathbf{r}_N + \mathbf{r}_N \cdot \mathbf{C}_\rho \cdot \mathbf{r}_N + \ldots, \tag{A1}$$

where b_ρ is a scalar, $\boldsymbol{B}_\rho$ and $\boldsymbol{C}'_\rho$ are vectors, and $\mathbf{C}_\rho$ is a 3×3 matrix. This includes analytic and nonanalytic terms. We may rewrite this as

$$\rho(\mathbf{r}) = \rho_{0,N} e^{-2Z r_N} + \rho_{\mathrm{smooth}}(\mathbf{r}), \tag{A2}$$

$$\rho_{\mathrm{smooth}}(\mathbf{r}) = \boldsymbol{B}_\rho \cdot \mathbf{r}_N + r_N \boldsymbol{C}'_\rho \cdot \mathbf{r}_N + \mathbf{r}_N \cdot \mathbf{C}''_\rho \cdot \mathbf{r}_N + \ldots, \tag{A3}$$

where $Z = -b_\rho/[2\rho_{0,N}]$ and $\mathbf{C}''_\rho = \mathbf{C}_\rho - 2Z^2\mathbf{I}$. Here we focus on a single nucleus: the smooth density must have a similar expansion near every nucleus.

We therefore obtain,

$$\frac{\nabla^2 \rho(\mathbf{r})}{\rho(\mathbf{r})} = \frac{-4Z}{r_N} + \frac{2\boldsymbol{C}'_\rho}{\rho_{0,N}} \cdot \hat{\mathbf{r}}_N + \mathrm{const.}, \tag{A4}$$

where $\hat{\mathbf{r}}$ indicates a unit vector. Clearly, the first term dominates and the second has a radial average of zero. This is how the cusp gives rise to singularities.

The nonsingular part, v_{nonsing}, of the potential obeys,

$$\lim_{\mathbf{r}\to\mathbf{R}_N} r_N v_{\mathrm{nonsing}}(\mathbf{r}) = 0, \quad \forall \mathbf{R}_N, \tag{A5}$$

and contains similar terms to Eq. (A3). It can also have a constant term, a term $B_v r_N$, and even logarithmic singularities like $L_v \log(r_N)$. Any nonsingular potential obeying Eq. (A5) will not alter any of the conclusions of the main text.

APPENDIX B: CUSPS LEAD TO SINGULARITIES

For two or few electrons it is trivial to show that singularities lead to cusps. The leading terms of our density may be described using $\rho := e^{-2Z_N r_N}$, where $\mathbf{r}_N = \mathbf{r} - \mathbf{R}_N$ is the distance from the cusp at $\mathbf{R}_N$. The remaining terms begin (by

definition) at $O(\mathbf{r}_N)$ and therefore contribute to the potential only at a constant or higher terms.

The nontrivial part of the von Weizsäcker potential is therefore the part involving only radial derivatives

$$v^{\mathrm{vW}} = \frac{\partial_{rr}\rho}{4\rho} + \frac{\partial_r \rho}{2r\rho} - \frac{(\partial_r \rho)^2}{8\rho^2} = \frac{Z_N^2}{2} - \frac{Z_N}{r}, \tag{B1}$$

which is clearly dominated by the $\frac{-Z_N}{r_N}$ singularity. This gives our proof for two electrons. To go beyond two electrons, we show that v^{vW} has the same singularities as the KS potential for more than two electrons.

To begin, rewrite $\rho = \sum_i f_i |\phi_i|^2$, [Eq. (3)] using

$$\zeta_i(\mathbf{r})\sqrt{\rho(\mathbf{r})} := \sqrt{f_i}\phi_i(\mathbf{r}), \tag{B2}$$

where $\sum_i |\zeta_i(\mathbf{r})|^2 = 1 \forall \mathbf{r}$, by definition. The KS orbital equations Eq. (1) yield $[\hat{h} - \epsilon_i]\phi_i = 0$, giving

$$\begin{aligned} 0 &= \frac{\sqrt{f_i}}{\sqrt{\rho}}\left[\frac{-\nabla^2}{2} + v_{\mathrm{KS}}[\rho] - \epsilon_i\right]\phi_i \\ &= \frac{1}{\sqrt{\rho}}\left[\frac{-\nabla^2}{2} + v_{\mathrm{KS}}[\rho] - \epsilon_i\right]\zeta_i\sqrt{\rho} \\ &= \left[\frac{-\nabla^2}{2} - \boldsymbol{g}[\rho]\cdot\nabla + \tilde{v}[\rho] - \delta_i\right]\zeta_i(\mathbf{r}), \end{aligned} \tag{B3}$$

for ζ_i. Here $\tilde{v} := v_{\mathrm{KS}}[\rho] - v^{\mathrm{vW}}[\rho]$, $\boldsymbol{g}[\rho] := \frac{\nabla\sqrt{\rho}}{\sqrt{\rho}} = \frac{\nabla\rho}{2\rho}$, and δ_i are constants.

Importantly, we recognize that $|\boldsymbol{g}| < \infty$ and is smooth in any nuclear density. Since δ_i is a constant, it follows that only differences in the location or magnitude of singularities in v_{KS} and v^{vW}, which manifest in $\tilde{v}$, can contribute to cusps in ζ_i. We denote the set of effective "nuclei" for which $\tilde{v}$ has singularities by $\tilde{\mathcal{C}} = \{(\mathbf{R}_N, z_N)\}$, with locations $\mathbf{R}_N$ and effective charges $z_N \neq 0 \forall N \in \tilde{\mathcal{C}}$ (we allow $z_N < 0$ for repulsive effective nuclei). Only these singularities may lead to cusps in ζ_i.

We next recognize that all singularities in $\tilde{v}$ give rise to cusps or zero solutions in ζ_i, which follows from the series expansion of Eq. (B3) on $r_N = |\mathbf{r} - \mathbf{R}_N|$ (see the discussion in the previous Appendix). Thus, to leading orders, we may define a set $\zeta_{i\in \boldsymbol{I}_c} \approx \zeta_{i,0}[1 - z_N r_N]$ with cusps and a complementary set $\zeta_{i\notin \boldsymbol{I}_c} \approx 0$ without cusps that are zero at the nuclei. However, by construction we find $1 = \sum_i |\zeta_i|^2 \approx \sum_{i\in \boldsymbol{I}_c} |\zeta_{i,0}|^2 - 2z_N r_N \sum_{i\in \boldsymbol{I}_c} |\zeta_{i,0}|^2 = C_N - 2z_N r_N C_N$ where $C_N = \sum_{i\in \boldsymbol{I}_N} |\zeta_{i,0}|^2$. This equation can only be simultaneously correct for leading and subleading order terms if $z_N = 0$, i.e., if there is no singularity in the vicinity of nucleus $\mathbf{R}_N$.

Since $z_N = 0$ for all nuclei N, it follows that $\tilde{\mathcal{C}}$ must be the empty set and that $\tilde{v}$ has no singularities. The KS potential v_{KS} therefore has the same singularities as the von Weizsäcker potential v^{vW} per Eq. (B1). This extends results to more than two electrons and yields

$$\sum_N \rho_{0,N} e^{-2Z_N r_N} \longrightarrow \sum_N \frac{-Z_N}{|\mathbf{r} - \mathbf{R}_N|}. \tag{B4}$$

[1] T. A. Wesolowski, S. Shedge, and X. Zhou, Frozen-density embedding strategy for multilevel simulations of electronic structure, Chem. Rev. **115**, 5891 (2015).

[2] Q. Sun and G. K.-L. Chan, Quantum embedding theories, Acc. Chem. Res. **49**, 2705 (2016).

[3] C. M. Isborn, A. W. Götz, M. A. Clark, R. C. Walker, and T. J. Martínez, Electronic absorption spectra from MM and *ab initio* QM/MM molecular dynamics: Environmental effects on the absorption spectrum of photoactive yellow protein, J. Chem. Theory Comput. **8**, 5092 (2012).

[4] T. A. Barnes, J. W. Kaminski, O. Borodin, and T. F. Miller, Ab initio characterization of the electrochemical stability and solvation properties of condensed-phase ethylene carbonate and dimethyl carbonate mixtures, J. Phys. Chem. C **119**, 3865 (2015).

[5] A. Schulz and C. R. Jacob, Description of intermolecular charge transfer with subsystem density-functional theory, J. Chem. Phys. **151**, 131103 (2019).

[6] H. Ma, M. Govoni, and G. Galli, Quantum simulations of materials on near-term quantum computers, npj Comput. Mater. **6**, 1 (2020).

[7] C. E. Starrett and D. Saumon, Electronic and ionic structures of warm and hot dense matter, Phys. Rev. E **87**, 013104 (2013).

[8] T. A. Wesolowski and A. Warshel, Frozen density functional approach for ab initio calculations of solvated molecules, J. Phys. Chem. **97**, 8050 (1993).

[9] T. A. Wesołowski, Embedding a multideterminantal wave function in an orbital-free environment, Phys. Rev. A **77**, 012504 (2008).

[10] K. Pernal and T. A. Wesolowski, Orbital-free effective embedding potential: Density-matrix functional theory case, Int. J. Quantum Chem. **109**, 2520 (2009).

[11] P. Cortona, Self-consistently determined properties of solids without band-structure calculations, Phys. Rev. B **44**, 8454 (1991).

[12] P. Elliott, K. Burke, M. H. Cohen, and A. Wasserman, Partition density-functional theory, Phys. Rev. A **82**, 024501 (2010).

[13] J. Nafziger and A. Wasserman, Density-based partitioning methods for ground-state molecular calculations, J. Phys. Chem. A **118**, 7623 (2014).

[14] M. Banafsheh and T. A. Wesolowski, Nonadditive kinetic potentials from inverted Kohn–Sham problem, Int. J. Quantum Chem. **118**, e25410 (2018).

[15] T. A. Wesolowski and A. Savin, Non-additive kinetic energy and potential in analytically solvable systems and their approximated counterparts, in *Recent Progress in Orbital-Free Density Functional Theory*, edited by T. A. Wesolowski and Y. A. Wang (World Scientific, Singapore, 2013), pp. 275–295.

[16] T. A. Wesolowski, H. Chermette, and J. Weber, Accuracy of approximate kinetic energy functionals in the model of Kohn-Sham equations with constrained electron density: The FH···NCH complex as a test case, J. Chem. Phys. **105**, 9182 (1996).

[17] T. A. Wesolowski, Density functional theory with approximate kinetic energy functionals applied to hydrogen bonds, J. Chem. Phys. **106**, 8516 (1997).
[18] E. Smargiassi and P. A. Madden, Orbital-free kinetic-energy functionals for first-principles molecular dynamics, Phys. Rev. B **49**, 5220 (1994).
[19] C. Huang and E. A. Carter, Nonlocal orbital-free kinetic energy density functional for semiconductors, Phys. Rev. B **81**, 045206 (2010).
[20] V. V. Karasiev, T. Sjostrom, and S. Trickey, Finite-temperature orbital-free DFT molecular dynamics: Coupling Profess and Quantum Espresso, Comput. Phys. Commun. **185**, 3240 (2014).
[21] K. Luo, V. V. Karasiev, and S. B. Trickey, A simple generalized gradient approximation for the noninteracting kinetic energy density functional, Phys. Rev. B **98**, 041111(R) (2018).
[22] X. Shao, W. Mi, and M. Pavanello, Revised Huang-Carter nonlocal kinetic energy functional for semiconductors and their surfaces, Phys. Rev. B **104**, 045118 (2021).
[23] K. Ryczko, S. J. Wetzel, R. G. Melko, and I. Tamblyn, Toward orbital-free density functional theory with small data sets and deep learning, J. Chem. Theory Comput. **18**, 1122 (2022).
[24] P. de Silva and T. A. Wesolowski, Exact non-additive kinetic potentials in realistic chemical systems, J. Chem. Phys. **137**, 094110 (2012).
[25] A. Savin and T. A. Wesolowski, Orbital-free embedding effective potential in analytically solvable cases, in *Advances in the Theory of Atomic and Molecular Systems* (Springer, New York, 2009), pp. 311–326.
[26] S. Fux, C. R. Jacob, J. Neugebauer, L. Visscher, and M. Reiher, Accurate frozen-density embedding potentials as a first step towards a subsystem description of covalent bonds, J. Chem. Phys. **132**, 164101 (2010).
[27] J. M. García-Lastra, J. W. Kaminski, and T. A. Wesolowski, Orbital-free effective embedding potential at nuclear cusps, J. Chem. Phys. **129**, 074107 (2008).
[28] E. Polak, C. E. González-Espinoza, M. J. Gander, and T. A. Wesolowski, A non-decomposable approximation on the complete density function space for the non-additive kinetic potential, J. Chem. Phys. **156**, 044103 (2022).
[29] E. Steiner, Charge densities in atoms, J. Chem. Phys. **39**, 2365 (1963).
[30] S. Liu, R. G. Parr, and A. Nagy, Cusp relations for local strongly decaying properties in electronic systems, Phys. Rev. A **52**, 2645 (1995).
[31] T. Kato, On the eigenfunctions of many-particle systems in quantum mechanics, Commun. Pure Appl. Math. **10**, 151 (1957).
[32] A. Nagy and K. Sen, Higher-order cusp of the density in certain highly excited states of atoms and molecules, J. Phys. B: At. Mol. Opt. Phys. **33**, 1745 (2000).
[33] R. T. Pack and W. B. Brown, Cusp conditions for molecular wavefunctions, J. Chem. Phys. **45**, 556 (1966).
[34] J. J. Bekx, S.-K. Son, B. Ziaja, and R. Santra, Electronic-structure calculations for nonisothermal warm dense matter, Phys. Rev. Res. **2**, 033061 (2020).
[35] V. V. Karasiev and S. X. Hu, Unraveling the intrinsic atomic physics behind x-ray absorption line shifts in warm dense silicon plasmas, Phys. Rev. E **103**, 033202 (2021).
[36] C. F. v. Weizsäcker, Zur theorie der kernmassen, Z. Phys. **96**, 431 (1935).
[37] R. G. Parr and W. Yang, *Density-Functional Theory of Atoms and Molecules* (Oxford University Press, Oxford, 1994).
[38] R. G. Gordon and Y. S. Kim, Theory for the forces between closed-shell atoms and molecules, J. Chem. Phys. **56**, 3122 (1972).
[39] C. R. Jacob, Unambiguous optimization of effective potentials in finite basis sets, J. Chem. Phys. **135**, 244102 (2011).
[40] Y. Shi and A. Wasserman, Inverse Kohn-Sham density functional theory: Progress and challenges, J. Phys. Chem. Lett. **12**, 5308 (2021).
[41] N. Helbig, I. V. Tokatly, and A. Rubio, Exact Kohn-Sham potential of strongly correlated finite systems, J. Chem. Phys. **131**, 224105 (2009).
[42] N. H. March, I. A. Howard, A. Holas, P. Senet, and V. E. Van Doren, Nuclear cusp conditions for components of the molecular energy density relevant for density-functional theory, Phys. Rev. A **63**, 012520 (2000).
[43] D. J. Bicout and M. J. Field, Stochastic dynamics simulations of macromolecular diffusion in a model of the cytoplasm of escherichia coli, J. Phys. Chem. **100**, 2489 (1996).
[44] P. Hohenberg and W. Kohn, Density functional theory (DFT), Phys. Rev. **136**, B864 (1964).
[45] W. Kohn, Density Functional and Density Matrix Method Scaling Linearly with the Number of Atoms, Phys. Rev. Lett. **76**, 3168 (1996).
[46] T. A. Wesolowski, Is the non-additive kinetic potential always equal to the difference of effective potentials from inverting the Kohn-Sham equation? J. Chem. Phys. **157**, 081102 (2022).
[47] A. Makmal, S. Kümmel, and L. Kronik, Fully numerical all-electron solutions of the optimized effective potential equation for diatomic molecules, J. Chem. Theory Comput. **5**, 1731 (2009).
[48] R. Garrick, A. Natan, T. Gould, and L. Kronik, Exact Generalized Kohn-Sham Theory for Hybrid Functionals, Phys. Rev. X **10**, 021040 (2020).
[49] B. Fornberg, Generation of finite difference formulas on arbitrarily spaced grids, Math. Comp. **51**, 699 (1988).
[50] T. L. Beck, Real-space mesh techniques in density-functional theory, Rev. Mod. Phys. **72**, 1041 (2000).
[51] J. R. Chelikowsky, N. Troullier, and Y. Saad, Finite-difference-pseudopotential method: Electronic structure calculations without a basis, Phys. Rev. Lett. **72**, 1240 (1994).
[52] D. M. Ceperley and B. J. Alder, Ground State of the Electron Gas by a Stochastic Method, Phys. Rev. Lett. **45**, 566 (1980).
[53] J. P. Perdew and Y. Wang, Accurate and simple analytic representation of the electron-gas correlation energy, Phys. Rev. B **45**, 13244 (1992).
[54] See Supplemental Material at http://link.aps.org/supplemental/10.1103/PhysRevA.106.042812 for details of numerical parameters and precision.